Experimental study on interaction and coalescence of synchronized multiple bubbles

Cui, P.; Wang, Qian; Wang, SP; Zhang, A

DOI:
10.1063/1.4939007

Experimental study on interaction and coalescence of synchronized multiple bubbles

P. Cui[1, 2], Q. X. Wang[2]*, S. P. Wang[1], A. M. Zhang[1]

[1] College of Shipbuilding Engineering, Harbin Engineering University, 145 Nantong Street, Harbin, China

[2] School of Mathematics, University of Birmingham, Edgbaston, Birmingham, UK

Experiments are carried out on the interaction and coalescence of two, three and four bubbles with **approximately the same** sizes, distributed evenly and symmetrically. The bubbles are generated simultaneously by electric discharges, using an **in-house** designed series circuit, and their interaction is captured using a high-speed camera. Particular attentions are paid to if/when coalescence of bubbles happens, and the motion of the joined bubbles. Some new features are observed, which depend mainly on the dimensionless distance $\gamma_{bb} = d_{bb}/R_{max}$, where d_{bb} is the inter-bubble distance and R_{max} is the maximum bubble radius. For $\gamma_{bb} > 2$, a jet forms and penetrates each side bubble, directed to the center of the configuration, resulting in a protrusion. Towards the end of collapse, a large portion of bubble gases is compressed into the protrusion from the main part of the toroidal bubble. For $\gamma_{bb} < 2$, the bubbles coalesce during expansion, and the part of the joined bubble's surface distal from the center of the configuration collapses faster than elsewhere. The experiments show that the oscillation period of multi-bubbles does not change appreciably without coalescence but increases significantly with coalescence. For three bubbles initiated at collinear positions with $\gamma_{bb} > 2$, the jets that form from the side bubbles are towards the middle, and the middle bubble splits into two parts, moving towards the two side bubbles. For $\gamma_{bb} < 2$, the side bubbles merge with the middle bubble during expansion, forming an ellipsoid bubble; the joined bubble collapses predominantly from two sides, where two inward jets **form** towards the end of collapse.

Key words: Bubble interaction; Bubble coalescence and split; Bubble jetting; Spark generated bubbles

1. Introduction

Bubble dynamics is receiving increasing attention due to its wide **range of** applications. Single-bubble dynamics has been intensively investigated during the past century theoretically [1-8], experimentally [9-14], and numerically [15-20]. The study on the interaction of multi-bubbles is much more challenging and associated with relatively **few studies** in the literature. In practice, however, bubbles tend to appear in clusters, clouds, filaments or groups, rather than in isolation [21-24], and the interactions between bubbles are therefore inevitable. This is true to a wide range of bubble applications, which includes not only the classic areas such as cavitation erosion [25, 26] and noise in hydraulic machinery [27-29], but also sonochemistry [30, 31], sonoluminescence [30, 32], ultrasonic cleaning [33-35] and seismic air-gun bubble arrays [36, 37], as well as medical applications including sonoporation [38, 39], ultrasound lithotripsy [40-42] and so on.

Experimental efforts have been made to study bubble interactions, using methods such as optical breakdown (laser) [43-47], electric discharge [48-50], small charge explosion [51], and pressure impulse [52]. Bubble interaction has also been studied with numerical methods such as the boundary integral method coupled with fast multiple expansions [53-56]. Recently, Han, et al.[57] studied bubble pairs with laser bubbles and the volume of fluid method.

This paper aims to study the interaction and coalescence of synchronically oscillating bubbles based on the following three considerations. Firstly, synchronic bubble interaction **is** associated with an important application for the air-gun clusters, which are used to generate a sound sources in seismic surveys. To explore complex geologies, low frequency acoustic waves are desirable, since the damping of acoustic energy is proportional to the square of frequencies [58]. In addition, low frequency acoustic waves usually are less harmful to marine mammals [59]. One possible method to reduce the acoustic frequency is to use airgun clusters to cause synchronized individual bubbles to coalesce into a bigger bubble [60, 61], which has a longer period.

Secondly, mutual interaction between bubbles tends to be stronger, if the bubbles have similar sizes and are evenly distributed; otherwise the interaction is dominated by larger bubbles and/or the relatively closer bubbles.

Thirdly, interaction between in-phase bubbles was less studied in previous experiments because it is difficult to generate bubbles at the same time and with the same size. Numerical studies in the literature are mostly focused on two bubbles in an axisymmetric configuration

[61] and simulations are carried out only till early stage of rebound. In both experiments and computations, behaviors of joined bubble formed by coalescence of multiple bubbles, such as collapse, rebound, split, jetting, and oscillation period of the joined bubble, were less concerned in previous works. Studies in these aspects are the aim of this paper.

In the present experimental study, a series circuit was employed in generating multiple bubbles with electric discharge. It ensures that approximately the same amount of energy is distributed to each bubble at the same time during the discharge; therefore the bubbles are generated simultaneously and oscillate synchronically to approximately the same maximum size. We carry out the following developments for two, three and four synchronized bubbles, focusing on coalescence of bubbles and the behaviors of the joined bubbles, as versus to the previous studies.

For two-bubble interaction, in-phase bubbles are known to migrate and jet towards each other [43, 44, 47, 50]; when out-of-phase, the bubble behaviors are more complex; jet direction changes and the bubbles may split [43, 44, 47-49, 62, 63]. Coalescence occurs if two bubbles are very close to each other [51, 63-65]. In this study, some new features in the interaction of two bubbles are observed with relatively small distance. In particular, we observed that a large portion of bubble gas contents may be compressed into a protrusion attached to the bubble, which is formed after jet penetration.

There are few studies in the literature for interaction of three bubbles. Khoo et al. [48] and Fong et al. [49] carried out a few cases for three bubbles, where the bubble behavior was complicated, due to a number of factors such as bubble phases, sizes and positions. The current experiment is capable of generating three evenly distributed synchronized bubbles of the same size. Thus, the mutual interaction will be stronger, and with the inter-bubble distance being the only parameter, bubble interaction patterns are categorized.

As for four or more interacting bubbles, bubbles placed at outer positions in a configuration were observed to migrate and collapse towards center bubbles when they are in-phase [45, 52, 66], while the bubbles were mostly shock wave induced and of relatively small scales in contrast to the current experiments. In this study, we will consider a new layout where four bubbles are located at the four vertexes of a virtual square with representative inter-bubble distances.

2. Experiment setup and measurements

In our experiment, bubbles are generated by low-voltage electric discharges. This method was initially introduced by Turangan et al. (2006) [67]. The discharge circuit in the current setup consists of a 200V DC supply, a 6600 μF capacitor, and a 1.0 kΩ resistor. The capacitor is charged to 200V before discharging, and the bubbles generated have relatively long periods (3-6 ms) and large radii (3-12 mm), providing convenience for observation. Copper alloy electrodes extending from the capacitor poles are crossed and touched at their other ends in water. The point where electrodes touch is referred to as a connect point. A bubble will be generated as a result of Joule heating at each connect point, when the discharge begins. Multiple connect points are placed at predefined locations to generate interacting bubbles in this experiment, and the connect points are regarded as the initial bubble centers.

The experiment setup is illustrated in figure 1. Bubbles are generated in a cubic glass tank with 0.5 m side length filled with water degassed by boiling. Images of bubbles are recorded by a Phantom V12.1 high-speed camera working at 20,000 frames per second (FPS). The water tank is illuminated by a 2kW spot light opposite to the camera through a diffuser (matte glass). The interval between two image frames is 50 μs, being small compared to the period of bubble oscillation (3-6 ms). Before discharging, a ruler placed besides the connect points is imaged as length calibration for captured images. The copper alloy wires are thin (0.12 mm in radius) compared to the bubble size; their influence to the bubble dynamics is expected to be small. The effects of the free surface and the glass tank walls are negligible, as they are located more than 20 times of maximum bubble radii away from the bubbles.

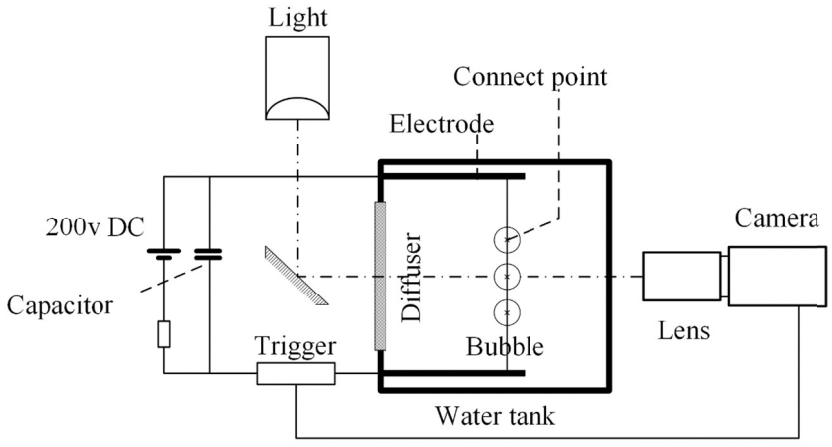

Figure 1. Experimental setup. Bubbles are generated at the connect points (crossed joints of thin copper alloy wires) with energy from the discharge of a capacitor. Bubble motions are captured with a high-speed camera working at 20,000 FPS. The water tank is lit up by continuous light through a diffuser.

The bubbles are incepted and expands due to the heating at the connect points during the discharge, with a bright light spot appearing at each connect point that are captured by the camera. In the multi-bubble experiments of Fong, et al. [49] and Khoo, et al. [48], the connect points of electrodes were embedded in parallel in the circuit. This made the heating at different inception points independent and ceasing at slightly different times; thus the bubble size and phase varied. In the present experiment, the connect points are deployed into a series circuit. Results show that the series circuit ensures firstly all light spots appear in the same image frame and thus the difference between the inception times for different bubbles is less than 50μs (i.e. the interval between two frames), and secondly all heating processes at different connect points cease at the same time and thus the expanding of all bubbles ends almost simultaneously. These characteristics make the bubbles in-phase and well synchronized.

The length scale is chosen as the maximum equivalent bubble radius R_{max}, and the time scale is the period T of the first cycle of oscillation. R_{max} is defined in terms of the area A of the 2D image of a bubble at its maximum expansion: $R_{max} = \sqrt{A/\pi}$. In experiments with multiple bubbles, corresponding average values are used.

3. Interaction of two synchronized bubbles

In the cases for two synchronized bubbles, we consider closer interactions as versus to previous studies [45, 48-50]. The dimensionless inter-bubble distance, γ_{bb}, is defined as,

$$\gamma_{bb} = \frac{d_{bb}}{R_{max}} \tag{1}$$

where d_{bb} is the distance between the bubble centers at inception. The dimensionless standoff distance of a bubble from a wall is

$$\gamma_{bw} = \frac{d_{bw}}{R_{max}} \tag{2}$$

where d_{bw} is the distance between the bubble center at inception and the wall. Figure 2 shows side by side a two-bubble case at $\gamma_{bb} = 2.6$ (frames 1-10) and a comparative case for a single bubble near a wall at $\gamma_{bw} = 1.3$ (frames a-j). Bubble shapes are provided at approximately equal dimensionless times, t_*, in terms of the first period of the corresponding bubble.

In frames 1-10, the bubbles oscillate nearly spherically to the late stage of collapse (frames 1-5), **when they move to the center of the configuration. This is due to the fact that the liquid flow to the inner side of each of the collapsing bubbles is retarded by the other collapsing bubble, and hence the distal sides of the two bubbles collapse faster. As a consequence of this motion,** two jets form on the distal sides of the two bubbles' surfaces and are directed towards the center of the configuration (frame 6).

The development of the jets can also be explained in terms of the Kelvin impulse [68, 69]. The virtual mass induced by the fluid flow around the bubble decreases gradually as the bubble shrinks in volume, while the Kelvin impulse approaches a constant value; therefore the velocity of the bubble wall distal from the center of configuration has to exceed that on the other side of the bubble wall. Consequently, the liquid on the far side of each bubble accelerate and focus, leading to the jet formation.

The jets have already pierced through the bubbles, before the bubble shrinks to their minimum volumes, see frames 6-7. In the in-phase two-bubble experiments at $\gamma_{bb} \approx 3.0$-5.0 [45, 48-50], however, the bubble jets did not develop until the very end of collapse and were not identified until bubble rebounding. In our experiments the bubbles are in a closer interaction, **the retardation effect of one bubble on the other bubble is stronger, and** jets are formed earlier and clearly indicated on the images (for example by the protrusions on bubble surface towards the jet directions).

After impacting on the opposite bubble walls, the two jets push the bubble walls ahead, generating two protrusions moving towards each other (frames 7-8). The protrusion is not likely to be a jet or part of a jet, since a jet should be of round tip due to surface tension and viscous shear stress, but the protrusions are with flat front in the images. We suggest that the protrusion should be a part of the toroidal bubble, with a necking **between it and the main part** of the toroidal bubble, as illustrated in figure 3. The jet penetrates through both the bubble and the protrusion with a rounded tip ahead of the protrusion, while the tip is invisible in the images. **The generation of the protrusion is explained as follows. After piercing through the bubble, the jet penetrates through the liquid on the opposite side of the**

bubble. Due to viscosity, it drags the liquid around the jet surface to flow along the jet direction. As a result, the bubble gases, around the exiting jet surface, flows with the liquid flow around the jet surface, resulting in a protrusion.

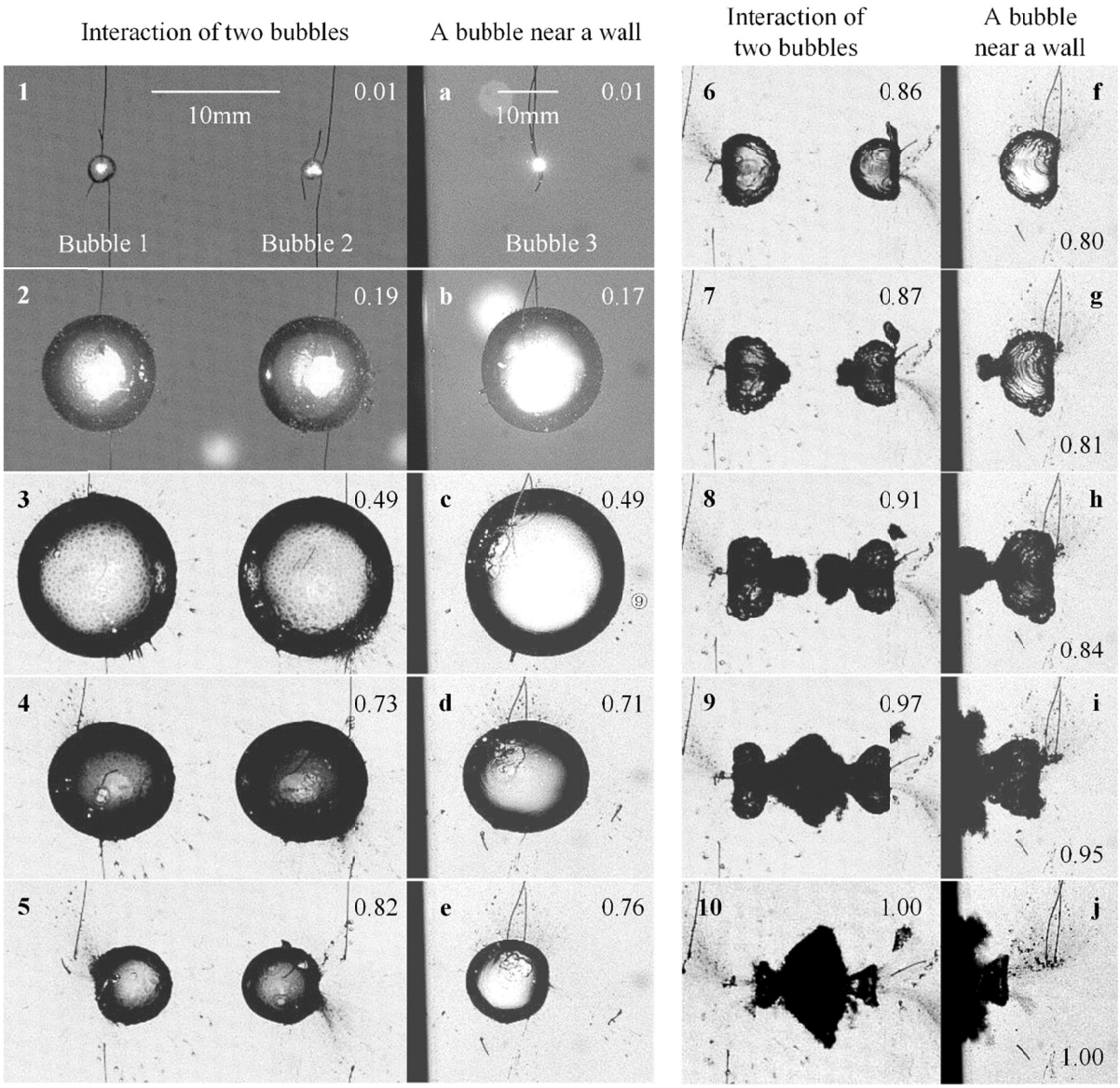

Figure 2. Frames 1-10 (columns 1 and 3 counting from left to right): interaction of two synchronized bubbles for the dimensionless inter-bubble distance $\gamma_{bb} = 2.6$. Frames a-j (the comparative case, columns 2 and 4): a single bubble near a wall for the dimensionless standoff distance $\gamma_{bw} = 1.3$. The dimensionless time t^* of each frame is marked on the corner. t^* increases from 0 to 1 during the first cycle of bubble oscillation. Length scales are shown in frames 1 and a.

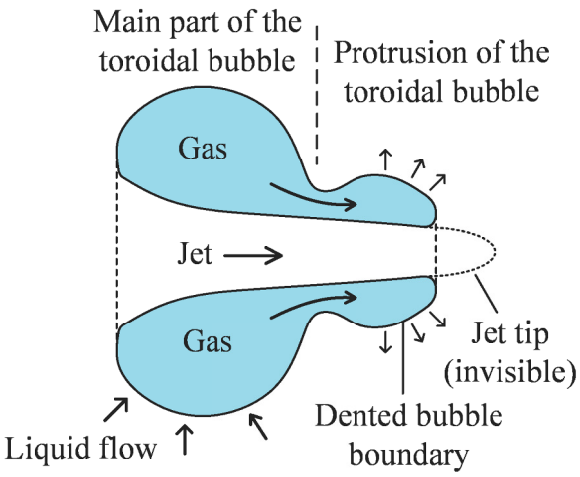

Figure 3. The structure of a protrusion formed after a jet penetrating a bubble (based on frame 8, figure 2). The filled area indicates the central section of the toroidal bubble along the jet direction. The protrusion is a part of the toroidal bubble, with a neck **connecting** it **with** the main part of the toroidal bubble. The jet penetrates through both of them with presumably a rounded tip ahead of the protrusion, but the tip is invisible in the images. The gases in the main part of the bubble are subsequently compressed into the protrusion (see frame 9, figure 2).

Interestingly, in frames 7-10, the main part of the toroidal bubble undergoes a rapid shrink in volume in a way that 'squeezes' its contents into the protrusion. **This phenomenon is explained as follows. A lower pressure zone is generated between two bubbles due to the pulling of liquid by both collapsing bubbles. The higher pressures at two sides of the configuration drive the two bubbles to move towards the center, and compress the gases from the main part of each toroidal bubble into its protrusion. The joining of the main part and the protrusion is with a higher velocity of the gas flow and thus a lower pressure according to Bernoulli's theorem, and becomes a neck compressed by the surrounding liquid. Our experiments show that a protrusion always forms after a bubble jet penetrates the bubble.**

In the comparative single-bubble case in frames a-j, where $\gamma_{bw} = 1/2\gamma_{bb}$, very similar bubble motion to the two-bubble case in frames 1-10 is shown at corresponding dimensionless times. A quantitative comparison of bubble motions is depicted in figure 4. The displacement-time curves of the leftmost point (LP) and rightmost point (RP) on bubble boundary are drawn, from bubble inception to the end of the first oscillation period, for two bubbles, i.e. one of the bubbles in the two-bubble case and the single bubble in the

comparative case. The displacement is defined as the horizontal distance from the point considered to the initial bubble center. When the jet penetrates the bubble, the two points join and the curves cross each other, as shown in the figure. The displacement curves in the two cases agree well in general, despite a slight delay in the motion of RP of the bubble from the two-bubble case during the late collapse stages (i.e. during jet development).

The resemblance between the two cases is expected. The reason behind is that the Reynolds number for the cases considered is high, the viscous effects are thus small and the method of image stands. In fact, the Reynolds number for the cases can be estimated as $O(10^3)$ using the maximum bubble radius (5-10mm) and jet speed (20-30 ms^{-1}) as the character length and velocity.

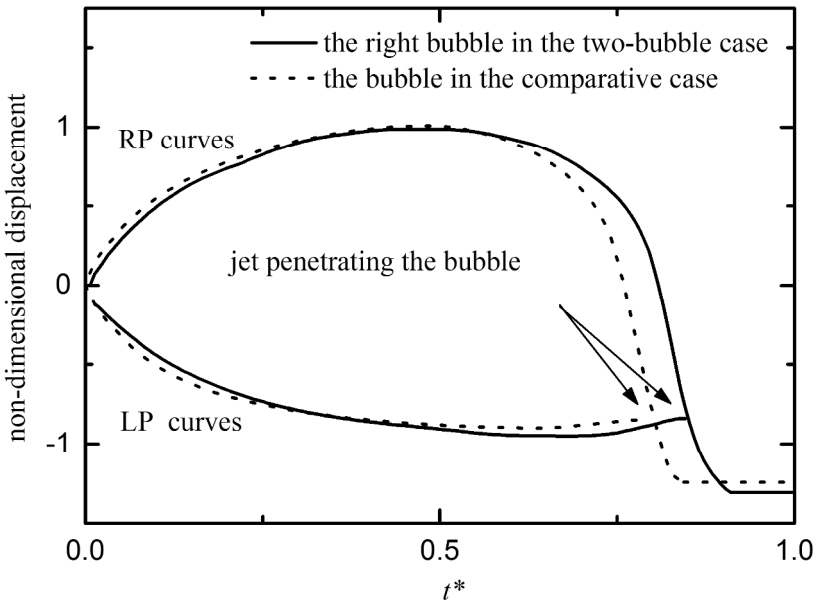

Figure 4. Dimensionless displacement-time curves for the leftmost point (LP) and rightmost point (RP) on bubbles' boundary. A comparison is made between the curves for the bubble on the right in the two-bubble case and the bubble in the bubble-wall case. The displacement is the horizontal distance measured from a bubble's initial centre to its LP or RP.

The other case for two bubbles, for $\gamma_{bb} = 0.8$, is shown in figure 5 (frames 1-6). The two bubbles start coalescing during the early stage of expansion (frames 2-3). The collapse of the joined bubble occurs mainly from its two distal sides (frames 4-6). This is because the bubble surfaces at two sides are associated with smaller curvature radii, and should collapse faster according to a proportional relationship between radius and Rayleigh collapse time [62].

The collapse pattern of either of the two bubbles is again very similar to that in the comparative case where there is no coalescence at all (shown in frames a-f).

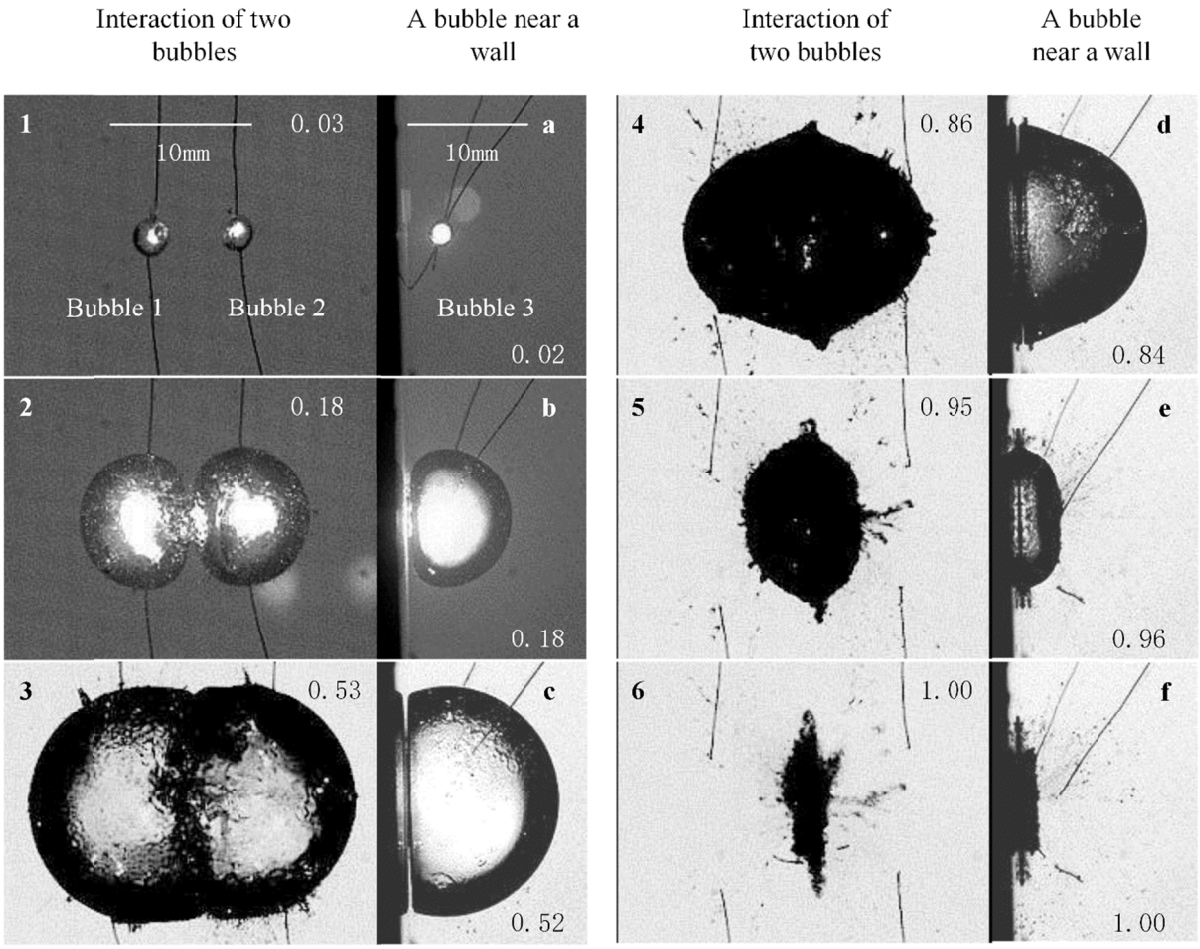

Figure 5. Frames 1-6: the interaction of two synchronized bubbles for the dimensionless inter-bubble distance $\gamma_{bb} = 0.8$. Frames a-f (the comparative case): a single bubble near a wall for the dimensionless standoff distance $\gamma_{bw} = 0.4$. The dimensionless time t_* of each frame is marked on the corner.

To analyze the increase of oscillation periods due to coalescence of bubbles, we introduce a dimensionless period T_{n*} for n joined bubbles,

$$T_{n*} = \frac{T_n}{R_{max}} \sqrt{\frac{p_\infty - p_v}{\rho}}, \tag{3}$$

where T_n is the period for n joined bubbles, p_∞, p_v and ρ are the ambient pressure, saturated vapor pressure and water density, respectively. R_{max} is the maximum radius of each bubble. Surface tension and viscous effects are negligible in the cases considered here, since the bubble radius is of $O(1)$ cm; therefore the period of bubble oscillation could be considered

proportional to the bubble's maximum radius [1, 70]. The bubble oscillation period is largely related to its volume and not affected significantly by its shape [71]. An empirical formula is thus provided for the oscillation period for n coalescing bubbles, based on the spherical bubble theory, as follows:

$$\frac{T_{n^*}}{T_{1^*}} = t_{*cls} + \left(1 - t_{*cls}\right)\sqrt[3]{n}\,, \tag{4}$$

where t_{cls*} is the dimensionless coalescence time, and $\boldsymbol{T_{1*}}$ **is the period for a single spherical bubble. We assume here that the bubbles have approximately the same sizes, collapse synchronically and coalesce at the same time.**

The first oscillation period for the two coalescing bubbles in figure 5 ends at frame 5. The dimensionless period T_{2*} in the experiment is 7.16, while the dimensionless period of a single bubble, T_{1*}, is 5.95. An increase of 20% is found with the coalescence. In figure 5, the coalescence starts at approximately 26% of the first oscillation, i.e. t_{cls*} = 0.26; hence by using (4), T_{2*} is supposed to be about 19% larger than T_{1*}. This estimation is close to the experimental result.

4. Interaction of three synchronized bubbles

In this section, we consider the interaction of three synchronized bubbles placed at collinear positions with equal inter-bubble distance. One of the interesting features noticed is the splitting of the bubble in the middle, which is observed in the case at γ_{bb} = 2.7, shown in figure 6. Since the phase difference is insignificant, the motion of the three-bubble configuration is symmetric. All the three bubbles oscillate approximately with a spherical shape to the middle stage of collapse. The two side bubbles are attracted by the middle bubble and moves towards **it** during collapse (frames 3-6). The far sides of the two side bubbles become flattened. In the meantime, the middle bubble is also attracted by the two side bubbles and thus becoming elongated (frames 3-6).

Afterwards, two jets form on the flattened far sides of the two side bubbles, directing to the middle bubble (frame 7). **This is due to the fact that the liquid flow to the inner side of a side bubble is retarded by the middle collapsing bubble.** The two jets develop rapidly, penetrate the two side bubbles and generate protrusions while the bubbles collapse (frames 7-10).

For the middle bubble, its two ends are attracted respectively by the two side bubbles. The middle cross-section of the middle bubble decreases obviously from frames 7 to 10, and a neck forms over there. **This is because that the liquid flows to the two sides of the middle bubble are retarded by the two collapsing side bubbles, the middle bubble thus collapses faster around its middle part. A lower pressure zone is generated between each side bubble and the middle bubble due to the pulling of liquid by the two collapsing bubbles.**

The middle bubble breaks up at its middle cross-section in frames 10-11**, as a result of the above-mentioned motion.** Each separated half of the middle bubble is attracted by and moves towards the corresponding side bubble (frames 11-13). **This should be caused by the lower pressure zone between each side bubble and the middle bubble, as well as a high pressure zone at the middle cross-section of the middle bubble, where a ring jet impacts to itself (frame 11). At the same time, the main part of the toroidal side bubble undergoes a rapid shrink in volume in a way that 'squeezes' its contents into its protrusion, as observed in the two bubble case in figure 3.** The protrusions **then** move towards the middle bubble **due to inertia**.

From frames 14 and onwards, the protrusion from the left bubble impacts and joins with the left half of the middle bubble, so does the protrusion from the right to the right half of the middle bubble. The two combinations **start a second cycle of expansion and collapses, during which they** are further attracted to each other and merge at the center of the configuration. In the meantime, the two side bubbles, which are toroidal and detached from the protrusions, move to the center too.

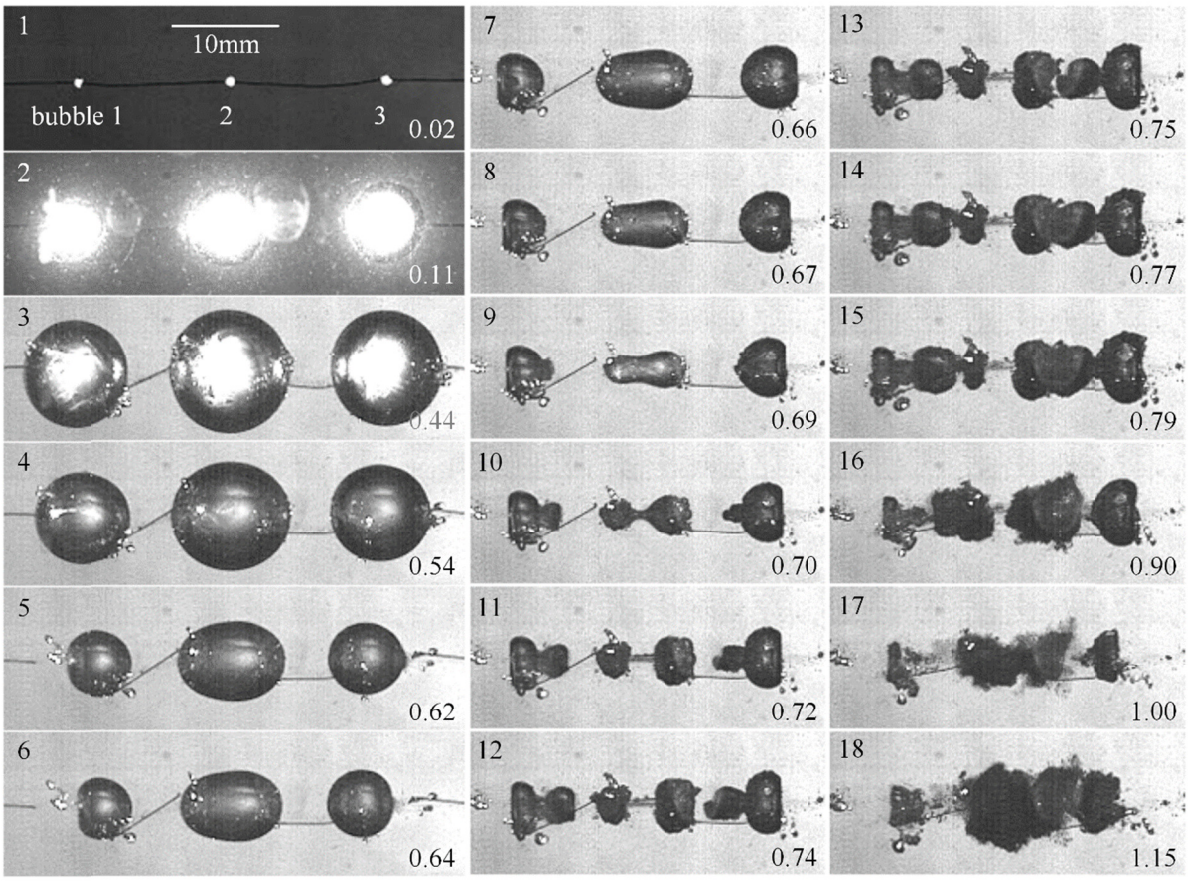

Figure 6. Interaction of three synchronized bubbles collinearly placed at equal dimensionless inter-bubble distance γ_{bb} = 2.7. The dimensionless time t_* of each frame is marked on the corner.

Another interesting pattern of three-bubble interaction is shown in figure 7, where γ_{bb} is reduced to 1.1. Due to the small inter-bubble distance, the three bubbles start squeezing each other since the early stage of expansion (frame 2 and onwards), **the liquid between bubbles rapidly drains, and the three bubbles coalesce. The far sides of the two side bubbles are not blocked and therefore** expand into hemi-spherical shapes, while the bubble in the middle, **being blocked at both sides**, grows into a cylindrical shape at the end of expansion (frame 4). The combined bubble takes an ellipsoid shape at this moment.

The joined bubble then collapses symmetrically (frames 4-12), predominantly from the two sides hemi-spherical faces, while its middle collapses slowly. As a result, the combined bubble becomes a circular cylinder with slightly larger cross-sections at the two ends. The above collapsing pattern of the joined bubble is interpreted as following. **T**he volume of each side bubble is approximately 87% of the center bubble right before joining (see frame 3). The inner pressure of the side bubbles is thus larger than that in the middle bubble. As a result, the

gases from both side bubbles flow to the center one once they joined (frame 4), **since the gases are highly compressible. The subtraction of gaseous contents from the two side bubbles leads to a greater difference between the inner pressure of the two side bubbles and the external liquid pressure, therefore a faster collapse of bubble boundaries at the two sides are expected.** The liquid flows following the gas flows from the two sides to the center further compress the two sides to make them flattened.

Two jets develop subsequently on the **left and right** ends of the joined bubble (i.e. from the hemi-spherical faces), **and the bubble continues collapsing. The concentration of the nearly incompressible liquid into a volume that becomes smaller and smaller accelerates the jet in the same direction of the collapse [72]. The jets** are clearly visible in frames 13 and 14. The jets penetrate through the middle bubble. The bubble collapses but remains in a circular cylinder profile, **with its length decreasing faster than the radius of its cross-section, since the bubble collapses faster from the two ends.**

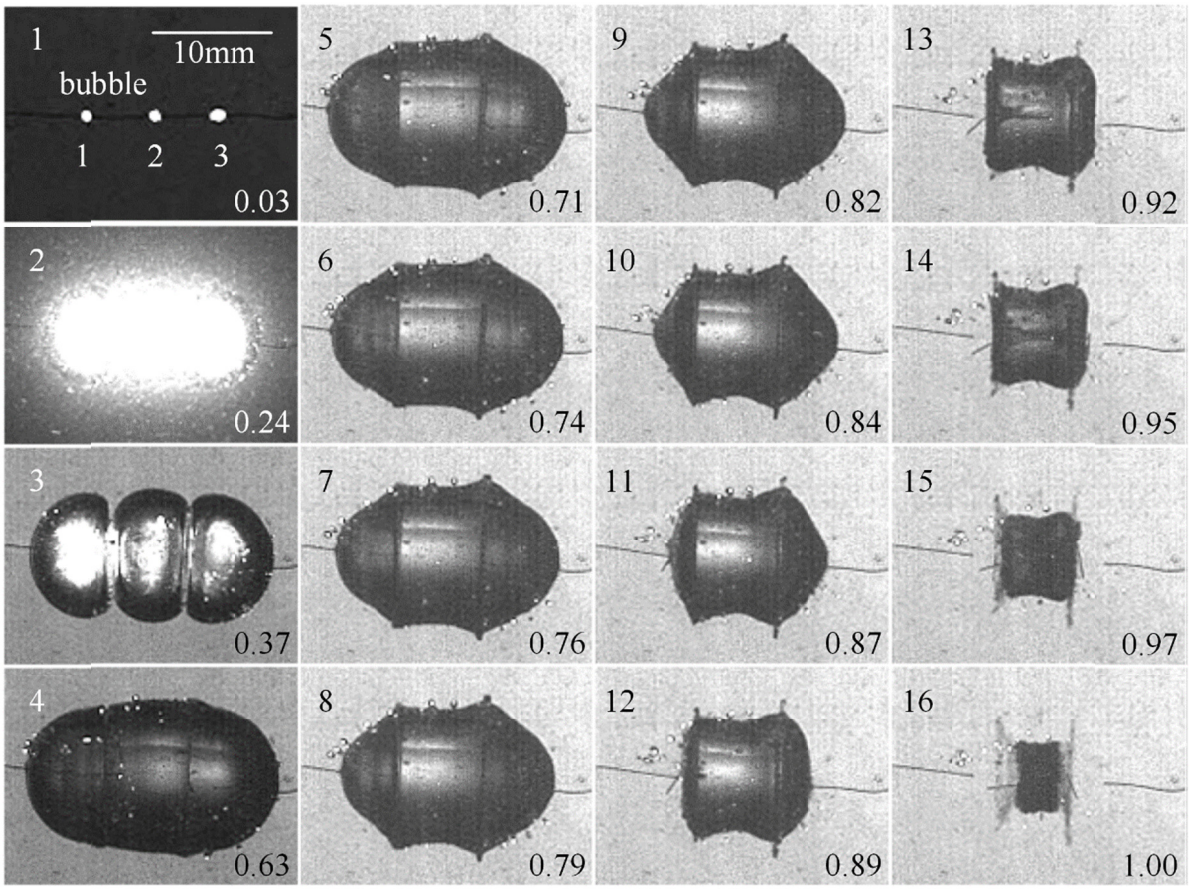

Figure 7. Interaction of three collinear synchronized bubbles at equal dimensionless inter-bubble distance γ_{bb} = 1.1. The dimensionless time t_* of each frame is marked on the corner.

5. Interaction of four synchronized bubbles

In the cases for four bubbles, the bubbles are located at the four vertexes of a square. The case for the dimensionless inter-bubble distance γ_{bb} = 3.1 is shown in figure 8 (frames 1-4). The bubbles expand almost spherically as they are not close to each other. The lower right bubble is smaller than the others due to uneven energy distribution in the circuit, but fortunately its phase differences to others are not substantial. Each of the bubbles moves to the center of the configuration **due to the combined second Bjerknes forces** from the other three bubbles **and develops a jet pointing to the same direction**. The bubbles are penetrated by the jets and become toroidal, before reaching their minimum volumes. Similar to the case for two bubbles in figure 2, protrusions form on the bubble surfaces close to the center of the configuration after the jets penetrate the bubbles. Each jet protrusion is pointing to the center and associated with a large part of the bubble gases (frame 4), which is similar to the case for two bubbles shown in figure 2.

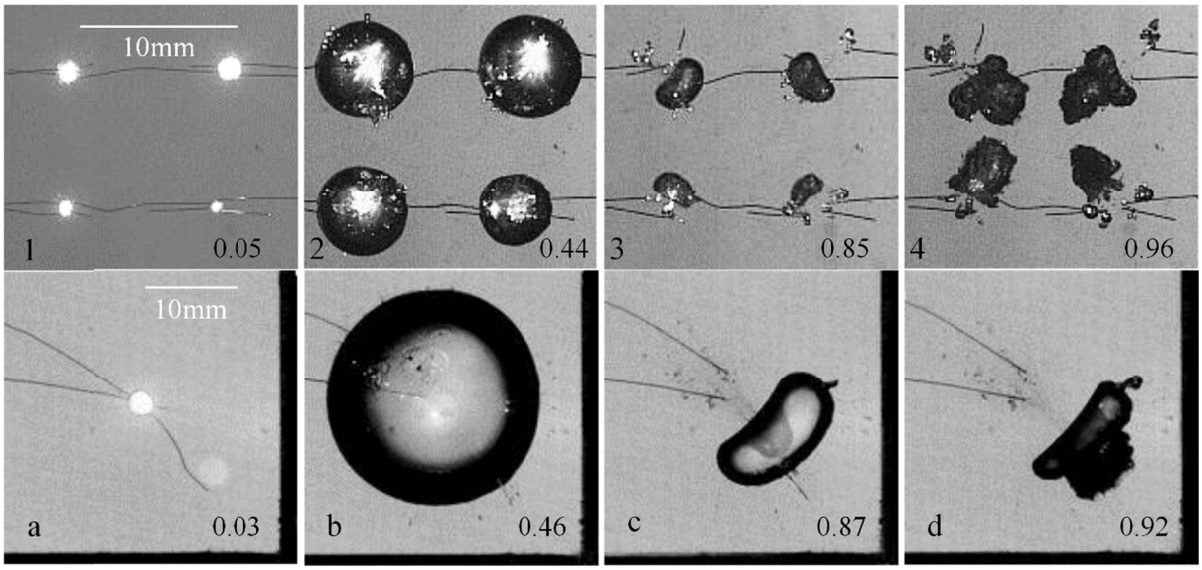

Figure 8. Upper row: interaction of four synchronized bubbles for the dimensionless inter-bubble distance γ_{bb} = 3.1. Lower row (the comparative case): motion of a single bubble near two perpendicular plane walls with the dimensionless standoff distance γ_{bw} = 1.54 from both walls. The dimensionless time t_* is marked on each frame.

In the comparative case shown along in frames a-d, a single bubble oscillates at the corner formed by two perpendicular plane walls. Here γ_{bw} is 1.54, approximately half of γ_{bb}. The motion of the bubble is very similar to the top-left bubble in the four-bubble case, especially when the bubble develops a re-entrant jet that penetrates it and causes a protrusion (frames c-d). As discussed in Section 3, this is because the viscosity effect is negligible due to the large Reynolds number associated. The two cases are equivalent based on the method of image.

Although the jet in the four bubble case is hardly visible, the jet in the comparative case shown in frame c is clear. The jet impinges on the opposite side of the bubble surface; a protrusion forms and the bubble becomes toroidal, as shown in frame d. As discussed in Section 3, the viscosity effects in these cases are negligible due to the large Reynolds number associated; therefore the four-bubble case and the comparative case are equivalent based on the method of image. The visualized jetting and other bubble behaviors in the comparative case can thus provide a relatively clear illustration of the motion of a bubble in the corresponding four-bubble system. The jetting should be pointing to the center of configuration for the case of four bubbles distributed evenly and symmetrically. This is confirmed by the comparative case.

Another case for a smaller inter–bubble distance, $\gamma_{bb} = 0.96$, is shown in figure 9, where the bubbles coalesce. The four bubbles expand to close contact in the middle stage of expansion (frame 2), and completely merge (frame 3) before reaching maximum volumes (frame 4). Interestingly, the joined bubble collapses predominantly at the parts that are further away from the center of configuration (see frames 3-5), **where are associated with smaller curvature radii. Lauterborn [62] argued that the bubble of a non-spherical bubble surface associated with a smaller local curvature radius collapses faster, since the collapsing speed of a spherical bubble is inverse to its radius according to the spherical bubble theory**. Finally the bubbles collapse to a minimum volume at the center. The behavior of each bubble is very similar to that of a single bubble near two perpendicular walls with $\gamma_{bw} = \gamma_{bb}/2$, as shown in the second row of figure 9 (the comparative case).

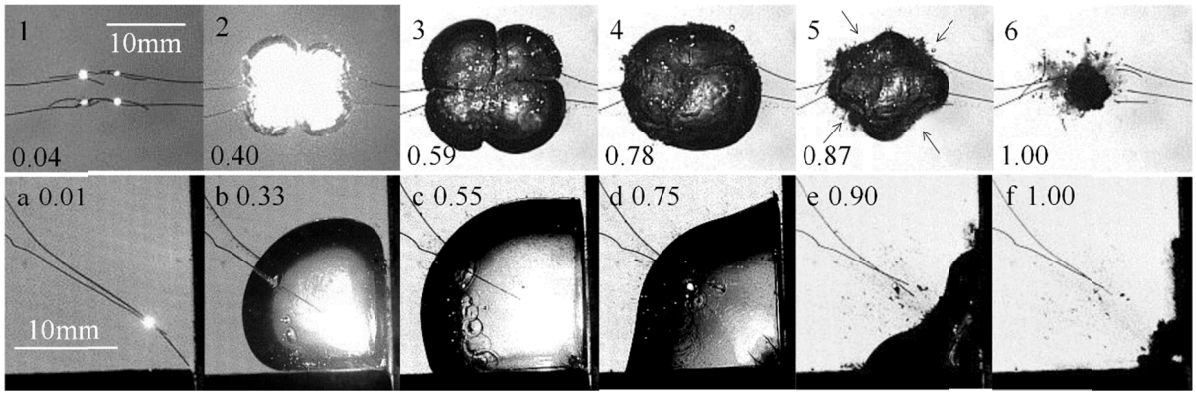

Figure 9. Frames 1-6: interaction of four synchronized bubbles for the dimensionless inter-bubble distance γ_{bb} = 0.96. Frames a-f (the comparative case): interaction between a single bubble and two perpendicular plane walls for the dimensionless standoff distance γ_{bw} = 0.48. The dimensionless time t_* of each frame is also marked on the images.

The dimensionless period for the four coalescing bubbles, T_{4*}, should be higher due to the increase in volume compared to one bubble. The increase is estimated as 47% compared to T_{1*} using (4), given that the coalescence occurred at 20% of the oscillation (i.e. t_{coal*} =0.20) in figure 9. Experimental result shows an increase of 52%, which agrees to the estimation.

6. Conclusions

This paper is concerned with the interaction of multiple synchronized bubbles with equal sizes, distributed evenly and symmetrically. The bubbles are generated simultaneously by electric discharges and their interactions are captured using a high-speed camera. We have verified that the method of image provides good approximation for symmetrical cases.

Some new features are observed and are summarized as follows, which depend mainly on the dimensionless distance $\gamma_{bb} = d_{bb}/R_{max}$, where d_{bb} is the inter-bubble distance and R_{max} is the maximum bubble radius.

For the cases with two or four bubbles, if $\gamma_{bb} > 2$, the bubbles are attracted to each other during oscillation by the second Bjerknes force. Before the end of collapse, each bubble that is not at the center of the configuration develops a jet; the jet form at the part of the bubble distal from the center of the configuration, and is pointing towards the center. After the jet penetrates and turns the bubble into toroidal, a protrusion is formed as part of the toroidal bubble, along the direction of the jet. The jet penetrates the protrusion too. A large

portion of bubble gases is compressed into the protrusion from the main part of the toroidal bubble, by the liquid flow following the migration and collapse of the bubble, and the main part of the toroidal bubble reduces in volume.

If $\gamma_{bb} < 2$, the bubbles coalesce during expansion. Then different parts on joined bubble surface collapse at different rates. The parts further from the center of the configuration collapse faster, and subsequently, jets form from there towards the center. The experiments show that the periods of oscillation of multiple bubbles do not change appreciably without coalescence but increase significantly with coalescence of bubbles. An empirical formula is provided for the oscillation period for *n* coalescing bubbles, based on the spherical bubble theory, which correlates with the experimental data. This demonstrates the mechanism of using airgun clusters to produce synchronized individual bubbles to coalesce into a bigger bubble, to generate a pressure wave at a large amplitude and a low frequency.

For the cases with three collinear bubbles, two patterns are displayed. If $\gamma_{bb} > 2$, the two side bubbles migrate and develop jets towards the middle bubble; the middle bubble becomes elongated due to the attraction from the two side bubbles and splits into two parts, which then join with the protrusions of the two side bubbles respectively. The two combinations are subsequently attracted to each other and merged at the center of the configuration. If $\gamma_{bb} < 2$, the three bubbles join. The joined bubble is ellipsoidal at maximum expansion, and then collapses predominantly from two sides. Two jets develop from the two sides and moves towards the center of the joined bubble. The collapse pattern is likely to be caused by a gas flux from the two side bubbles into the middle bubble after they merged, since the two side bubbles collapse faster than the middle one and has larger pressure before joining.

References

1. L. Rayleigh, "On the pressure developed in a liquid during the collapse of a spherical cavity," Philos Mag **34**, 94 (1917).
2. M. S. Plesset, and A. Prosperetti, "Bubble dynamics and cavitation," Annu Rev Fluid Mech **9**, 145 (1977).
3. Prosperetti, "Bubbles," Phys. Fluids **16**, 1852 (2004).
4. Z. C. Feng, and L. G. Leal, "Nonlinear bubble dynamics," Annu Rev Fluid Mech **29**, 201 (1997).
5. Z. Feng, and L. Leal, "Bifurcation and chaos in shape and volume oscillations of a periodically driven bubble with two-to-one internal resonance," J Fluid Mech **266**, 209 (1994).
6. Z. C. Feng, and L. G. Leal, "On energy transfer in resonant bubble oscillations," Physics of

Fluids A: Fluid Dynamics (1989-1993) **5**, 826 (1993).
7. S. Yang, Z. Feng, and L. Leal, "Nonlinear effects in the dynamics of shape and volume oscillations for a gas bubble in an external flow," J Fluid Mech **247**, 417 (1993).
8. I. Kang, and L. Leal, "Bubble dynamics in time-periodic straining flows," J. Fluid Mech **218**, 41 (1990).
9. C. F. Naudé, and A. T. Ellis, "On the Mechanism of Cavitation Damage by Nonhemispherical Cavities Collapsing in Contact With a Solid Boundary," J Fluids Eng **83**, 648 (1961).
10. Y. Tomita, and A. Shima, "Mechanisms of impulsive pressure generation and damage pit formation by bubble collapse," J Fluid Mech **169**, 535 (1986).
11. A. Philipp, and W. Lauterborn, "Cavitation erosion by single laser-produced bubbles," J Fluid Mech **361**, 75 (1998).
12. S. R. Gonzalez-avila, E. Klaseboer, B. C. Khoo, and C. Ohl, "Cavitation bubble dynamics in a liquid gap of variable height," J Fluid Mech **682**, 241 (2011).
13. E. A. Brujan, K. Nahen, P. Schmidt, and A. Vogel, "Dynamics of laser-induced cavitation bubbles near an elastic boundary," J Fluid Mech **433**, 251 (2001).
14. G. L. Chahine, "Interaction between an oscillating bubble and a free Surface," J Fluids Eng **99**, 709 (1977).
15. J. R. Blake, and D. C. Gibson, "Cavitation bubbles near boundaries," Annu Rev Fluid Mech **19**, 99 (1987).
16. E. Johnsen, and T. Colonius, "Numerical simulations of non-spherical bubble collapse," J Fluid Mech **629**, 231 (2009).
17. Q. X. Wang, and J. R. Blake, "Non-spherical bubble dynamics in a compressible liquid. Part 2. Acoustic standing wave," J Fluid Mech **679**, 559 (2011).
18. Q. X. Wang, and J. R. Blake, "Non-spherical bubble dynamics in a compressible liquid. Part 1. Travelling acoustic wave," J Fluid Mech **659**, 191 (2010).
19. G. A. Curtiss, D. M. Leppinen, Q. X. Wang, and J. R. Blake, "Ultrasonic cavitation near a tissue layer," J Fluid Mech **730**, 245 (2013).
20. C.-T. Hsiao, A. Jayaprakash, A. Kapahi, J.-K. Choi, and G. L. Chahine, "Modelling of material pitting from cavitation bubble collapse," J Fluid Mech **755**, 142 (2014).
21. R. F. Young, *Cavitation* (McGraw-Hill, 1989).
22. C. E. Brennen, *Cavitation and bubble dynamics* (Cambridge University Press, 2013).
23. T. Leighton, *The acoustic bubble* (Academic press, 1994).
24. E.-A. Brujan, and Y. Matsumoto, "Shock wave emission from a hemispherical cloud of bubbles in non-Newtonian fluids," J Non-newton Fluid **204**, 32 (2014).
25. C.-T. Hsiao, and G. L. Chahine, "Dynamic response of a composite propeller blade subjected to shock and bubble pressure loading," J Fluid Struct **54**, 760 (2015).
26. K.-H. Kim, G. Chahine, J.-P. Franc, and A. Karimi, *Advanced Experimental and Numerical Techniques for Cavitation Erosion Prediction* (Springer, 2014).
27. S. Li, "Cavitation enhancement of silt erosion—An envisaged micro model," Wear **260**, 1145 (2006).
28. Y. J. Zhang, S. C. Li, and F. G. Hammitt, "Statistical investigation of bubble collapse and cavitation erosion effect," Wear **133**, 257 (1989).
29. S. Li, Z. Zuo, S. Liu, Y. Wu, and S. Li, "Cavitation resonance," J Fluids Eng **130**, 031302 (2008).
30. C. D. Ohl, T. Kurz, R. Geisler, O. Lindau, and W. Lauterborn, "Bubble dynamics, shock waves and sonoluminescence," Philos T Roy Soc A **357**, 269 (1999).
31. K. M. Kalumuck, and G. L. Chahine, "The use of cavitating jets to oxidize organic compounds in water," J Fluids Eng **122**, 465 (2000).
32. E. A. Brujan, D. S. Hecht, F. Lee, and G. A. Williams, "Properties of luminescence from

laser-created bubbles in pressurized water," Phys Rev E **72**, 066310 (2005).
33. C.-D. Ohl, M. Arora, R. Dijkink, V. Janve, and D. Lohse, "Surface cleaning from laser-induced cavitation bubbles," Appl Phys Lett **89**, 074102 (2006).
34. D. Pavard, E. Klaseboer, S.-W. Ohl, and B. C. Khoo, "Removal of particles from holes in submerged plates with oscillating bubbles," Phys Fluids **21**, 083304 (2009).
35. G. L. Chahine, A. Kapahi, J.-K. Choi, and C.-T. Hsiao, "Modeling of Surface Cleaning by Cavitation Bubble Dynamics and Collapse," Ultrason Sonochem (2015).
36. F. Avedik, V. Renard, J. Allenou, and B. Morvan, ""“Single bubble” air-gun array for deep exploration," Geophysics **58**, 366 (1993).
37. A. Ziolkowski, G. Parks, L. Hatton, and T. Haugland, "The signature of an air-gun array: Computation from near-field measurements including interactions," Geophysics **47**, 1413 (1982).
38. C.-D. Ohl, M. Arora, R. Ikink, N. de Jong, M. Versluis, M. Delius, and D. Lohse, "Sonoporation from jetting cavitation bubbles," Biophys J **91**, 4285 (2006).
39. C.-D. Ohl, and B. Wolfrum, "Detachment and sonoporation of adherent HeLa-cells by shock wave-induced cavitation," Bba-gen Subjects **1624**, 131 (2003).
40. M. Arora, C. Ohl, and D. Lohse, "Effect of nuclei concentration on cavitation cluster dynamics," J Acoust Soc Am **121**, 3432 (2007).
41. E. Klaseboer, S. W. Fong, C. K. Turangan, and B. C. Khoo, "Interaction of lithotripter shockwaves with single inertial cavitation bubbles," J. Fluid Mech. **593**, 33 (2007).
42. M. Calvisi, J. Iloreta, and A. Szeri, "Dynamics of bubbles near a rigid surface subjected to a lithotripter shock wave. Part 2. Reflected shock intensifies non-spherical cavitation collapse," J Fluid Mech **616**, 63 (2008).
43. W. Lauterborn, and W. Hentschel, "Cavitation bubble dynamics studied by high speed photography and holography: part one.," Ultrasonics **23**, 260 (1985).
44. J. Blake, P. Robinson, A. Shima, and Y. Tomita, "Interaction of two cavitation bubbles with a rigid boundary," J Fluid Mech **255**, 707 (1993).
45. L. Werner, and K. Thomas, "Physics of bubble oscillations," Rep Prog Phys **73**, 106501 (2010).
46. P. Testud‐Giovanneschi, A. Alloncle, and D. Dufresne, "Collective effects of cavitation: Experimental study of bubble‐bubble and bubble‐shock wave interactions," J Appl Phys **67**, 3560 (1990).
47. Y. Tomita, A. Shima, and K. Sato, "Dynamic behavior of two-laser-induced bubbles in water," Appl Phys Lett **57**, 234 (1990).
48. B. C. Khoo, D. Adikhari, S. W. Fong, and E. Klaseboer, "Multiple spark-generated bubble interactions," Mod Phys Lett B **23**, 229 (2009).
49. S. W. Fong, D. Adhikari, E. Klaseboer, and B. C. Khoo, "Interactions of multiple spark-generated bubbles with phase differences," Exp Fluids **46**, 705 (2009).
50. E. F. Timm, and F. G. Hammit, "Bubble collapse adjacent to a rigid wall, a flexible wall, and a second bubble," ASME Cavitation Forum 18 (1971).
51. M. K. Lal, and S. Menon, "Interaction of two underwater explosion bubbles," ASME Fluids Engineering Divison Conference **236**, 595 (1996).
52. N. Bremond, M. Arora, C.-D. Ohl, and D. Lohse, "Controlled multibubble surface cavitation," Phys Rev Lett **96**, 224501 (2006).
53. Y. N. Zhang, and S. C. Li, "Direct numerical simulation of collective bubble behavior," Journal Of Hydrodynamics **22**, 785 (2010).
54. H. Chen, S. C. Li, Z. G. Zuo, and S. Li, "DIRECT NUMERICAL SIMUIATION OF BUBBLE-CLUSTER'S DYNAMIC CHARACTERISTICS," Journal Of Hydrodynamics **20**, 689 (2008).
55. G. L. Chahine, and R. Duraiswami, "Dynamical interactions in a multibubble cloud,"

ASME Journal of Fluid Engineering **114**, 680 (1992).
56. J. P. Best, "The formation of toroidal bubbles upon the collapse of transient cavities," J Fluid Mech **251**, 79 (1993).
57. B. Han, K. Köhler, K. Jungnickel, R. Mettin, W. Lauterborn, and A. Vogel, "Dynamics of laser-induced bubble pairs," J Fluid Mech **771**, 706 (2015).
58. G. Cambois, A. Long, G. Parkes, T. Lundsten, A. Mattsson, and E. Fromyr, *Multi-level airgun array: A simple and effective way to enhance the low frequency content of marine seismic data* (Society of Exploration Geophysicists, 2009).
59. A. N. Popper, M. E. Smith, P. A. Cott, B. W. Hanna, A. O. MacGillivray, M. E. Austin, and D. A. Mann, "Effects of exposure to seismic airgun use on hearing of three fish species," The Journal of the Acoustical Society of America **117**, 3958 (2005).
60. D. Barker, and M. Landrø, "Estimation of bubble time period for air-gun clusters using potential isosurfaces," Geophysics **78**, P1 (2013).
61. D. Barker, and M. Landrø, "Simple expression for the bubble-time period of two clustered air guns," Geophysics **77**, A1 (2012).
62. W. Lauterborn, "Cavitation bubble dynamics - new tools for an intricate problem," Appl Sci Res **38**, 165 (1982).
63. L. W. Chew, E. Klaseboer, S.-W. Ohl, and B. C. Khoo, "Interaction of two differently sized oscillating bubbles in a free field," Phys Rev E **84**, 066307 (2011).
64. K. Y. Lim, P. A. Quinto-Su, E. Klaseboer, B. C. Khoo, V. Venugopalan, and C.-D. Ohl, "Nonspherical laser-induced cavitation bubbles," Phys Rev E **81**, 016308 (2010).
65. S. Rungsiyaphornrat, E. Klaseboer, B. Khoo, and K. Yeo, "The merging of two gaseous bubbles with an application to underwater explosions," Comput Fluids **32**, 1049 (2003).
66. W. Lauterborn, T. Kurtz, R. Mettin, and C. D. Ohl, "Experimental and theoretical bubble dynamics," Adv Chem Phys **110**, 295 (1999).
67. C. K. Turangan, G. P. Ong, E. Klaseboer, and B. C. Khoo, "Experimental and numerical study of transient bubble-elastic membrane interaction," J Appl Phys **100**, 054910 (2006).
68. T. Benjamin, and A. T. Ellis, "The collapse of cavitation bubbles and the pressures thereby produced against solid boundaries," Philosophical Transactions Of The Royal Society Of London Series A-mathemat 221 (1966).
69. J. R. Blake, D. M. Leppinen, and Q. Wang, "Cavitation and bubble dynamics: the Kelvin impulse and its applications," Interface Focus **5**, 20150017 (2015).
70. M. S. Plesset, and R. B. Chapman, "Collapse of an initially spherical vapour cavity in the neighbourhood of a solid boundary," J Fluid Mech **47**, 283 (1971).
71. Y. X. Yang, Q. X. Wang, and T. Keat, "Dynamic features of a laser-induced cavitation bubble near a solid boundary," Ultrason Sonochem **20**, 1098 (2013).
72. A. Vogel, W. Lauterborn, and R. Timm, "Optical and acoustic investigations of the dynamics of laser-produced cavitation bubbles near a solid boundary," J Fluid Mech **206**, 299 (1989).